Carbohydrate Polymers 90 (2012) 1656–1663

Contents lists available at SciVerse ScienceDirect

Carbohydrate Polymers

journal homepage: www.elsevier.com/locate/carbpol

LBL structured chitosan-layered silicate intercalated composites based fibrous mats for protein delivery

Wei Li[a,1], Ruifen Xu[b,c,1], Liangqun Zheng[a,1], Jing Du[a], Yuli Zhu[a], Rong Huang[a], Hongbing Deng[a,*]

[a] College of Food Science and Technology and the MOE Key Laboratory of Environment Correlative Dietology, Huazhong Agricultural University, No. 1 Shizishan Road, Wuhan 430070, China
[b] Department of Anesthesiology, School of Stomatology, Fourth Military Medical University, Xi'an 710032, China
[c] School of Life Science and Technology, Xi'an Jiaotong University, Xi'an 710049, China

ARTICLE INFO

Article history:
Received 11 May 2012
Received in revised form 16 July 2012
Accepted 17 July 2012
Available online 25 July 2012

Keywords:
Chitosan
Organic rectorite
LBL
Fibrous mats
Protein delivery

ABSTRACT

Organic rectorite (OREC) was used to prepare intercalated composites with chitosan. The negatively charged cellulose acetate (CA) fibrous mats were modified with multilayers of the positively charged chitosan or chitosan–OREC intercalated composites and the negatively charged bovine serum albumin (BSA) via electrostatic layer-by-layer (LBL) self-assembly technique. The morphology and protein delivery properties of the resultant samples were investigated by regulating the number of deposition bilayers, the outermost layer and the composition of coating bilayers. The thickness of LBL films coated CA mats increased as the number of bilayers was increased and OREC was added. X-ray photoelectron spectroscopy indicated that chitosan and OREC were deposited on CA fibers. Small angle X-ray diffraction patterns showed that OREC was intercalated by chitosan. The *in vitro* BSA encapsulation and release experiments demonstrated that OREC could affect the degree of protein loading capacity and release efficiency of the LBL films coating.

1. Introduction

Nowadays, controlled release of protein-delivery systems has attracted extensive attention and become one of the most important goals for protein utilization. In the past decades, protein delivery systems have been developed by using polymeric materials in the form of reservoir system, microspheres, polymer matrices, hydrogel and others (Gonzalez-Rodriguez, Holgado, Sanchez-Lafuente, Rabasco, & Fini, 2002). At present, in the research field of drug-delivery systems, it has been concluded that drug-loaded electrospun fibers with higher drug encapsulation efficiency and better stability than other drug formulations (Tiwari, Tzezana, Zussman, & Venkatraman, 2010; Ma et al., 2011). In addition, polymeric delivery systems can stabilize proteins (Gonzalez-Rodriguez et al., 2002; Wu & Jin, 2008). Based on the previous studies, it is reasonable to hypothesize that the electrospun fibers with high surface-to-volume ratio and resultant accelerated solubility of protein in the aqueous solution as well as enhanced efficiency of protein (Deng, Wang, et al., 2011; Ma et al., 2011) will probably show great promise in the field of protein delivery in gastrointestinal tract.

As a protein carrier, the toxicity, biocompatibility and biodegradability are significant parameters to be considered (Xu et al., 2012; Zhang, Guo, Peng, & Jin, 2004). Therefore, some research efforts have been directed toward developing safe and efficient chitosan contained protein-delivery systems. Several biological properties of chitosan, such as the natural abundance, biodegradability, non-toxicity, biocompatibility, make it an attractive material for application in medical fields (Bhattarai, Edmondson, Veiseh, Matsen, & Zhang, 2005; Deng et al., 2010; Deng, Wang, et al., 2011). Besides, chitosan has a positive charge when it is dispersed in an aqueous solution system (Wang, Shi, Chen, & Baker, 2009).

In order to broaden its application in protein-delivery systems, some organic and inorganic materials have been considered to be incorporated with chitosan. Recently, polymer/layered silicate composites have attracted intensive attentions because they possess properties of both organic and inorganic materials (Darder, Colilla, & Ruiz-Hitzky, 2003; Deng, Wang, et al., 2011; Wang et al., 2006). Polymer/layered silicate composites can be good candidates as deposition materials to form LBL structured films to improve the properties of the templates. The previous studies reported that rectorite (REC), especially organic rectorite (OREC, modified from REC), might be more preferred because of their larger interlayer distance, better separable layer thickness and layer aspect ratio compared with regular layered silicates such as montmorillonite (Wang et al., 2006; Wang, Pei, Du, & Li, 2008; Wang, Shi, et al., 2009; Wang,

* Corresponding author. Tel.: +86 27 87282111; fax: +86 27 87282111.
E-mail address: alphabeita3000@yahoo.com.cn (H. Deng).
[1] Co-first author with the same contribution to this work.

0144-8617/$ – see front matter © 2012 Elsevier Ltd. All rights reserved.
http://dx.doi.org/10.1016/j.carbpol.2012.07.046

Tang, Li, Zhu, & Du, 2010), which might contribute to controlling the protein release in the mats. Moreover, chitosan–OREC intercalated composite was proved to be positively charged when it was dispersed in an aqueous solution system (Wang, Du, et al., 2009). Thus, chitosan–OREC can be expected to be used to make a potential protein-delivery system (Wang et al., 2010; Xu et al., 2012), and only few related researches on chitosan–OREC composites based fibrous mats have been done.

In this study, we fabricate chitosan–OREC composites with intercalated structure, and use them together with fibrous mats as protein delivery system to investigate whether OREC can enhance the loading capacity and improve the controlled release properties of the protein. As we know, chitosan–OREC composites are positively charged and protein is negatively charged. Therefore, bovine serum albumin (BSA) is selected as a model protein and electrostatic layer-by-layer (LBL) self-assembly technique is performed to alternatively immobilize BSA and chitosan–OREC composites on the surface of negatively charged cellulose acetate (CA) electrospun fibrous mats. LBL, introduced by Decher and Hong (1991), is a powerful and efficient method to form multilayer ultra-thin films on selected substrates with various shapes and sizes (Ding, Fujimoto, & Shiratori, 2005). The effect of the outermost layer variation, the number of deposition bilayers, and the composition of the multilayer on the formation of the LBL structured fibrous mats and the protein delivery properties of LBL films coating are investigated. Finally, the influence of OREC on the protein loading capacity and controlled release has also been studied.

2. Experimental details

2.1. Materials

Cellulose acetate (CA, $M_n = 3 \times 10^4$) was purchased from Sigma–Aldrich Co., USA. Chitosan (CS, $M_w = 2.0 \times 10^5$ kDa) from shrimp shell with 92% deacetylation was provided by Zhejiang Yuhuan Ocean Biochemical Co., China. Calcium rectorite (Ca^{2+}-REC) was supplied by Hubei Mingliu Inc., Co., China. Sodium alginate (ALG, 2.5×10^5 kDa) was from Aladdin Chemical Reagent Co., China. Bovine serum albumin (BSA, $M_w = 6.8 \times 10^4$ Da) was from Roche Diagnostics Co., USA. Coomassie Brilliant Blue (G250) was from Amresco Inc., USA. The other reagents were analytical grade. All aqueous solutions were prepared using purified water with a resistance of 18.2 MΩ cm.

2.2. Preparation of OREC and chitosan–OREC composites

The organic rectorite (OREC) and the intercalated chitosan–OREC composites were prepared according to our previous report (Deng, Li, et al., 2011; Deng et al., 2012). Briefly, the REC was dispersed in purified water to obtain the clay suspension under vigorous stirring for 30 min, and then left standing for 24 h. 2% sodium dodecylsulfonate (SDS) solution was added slowly into the above suspension at 90 °C with 5 h stirring. The resultant product was washed several times with purified water and filtered by decompress filter to remove excessive SDS. The sample was freeze-dried to yield OREC. Additionally, 2% chitosan solution was prepared by adding chitosan into 2% acetic acid with slow magnetic stirring in close vials for 2 h at room temperature, and then the prepared chitosan solution was added slowly into the pretreated OREC suspension with stirring at 60 °C for 2 days to obtain the composites with initial chitosan:OREC weight ratio of 12:1. The resulting mixture was then precipitated with 1 M NaOH. The formed composites were washed with distilled water until the solution became neutral. Finally, the chitosan–OREC composites were freeze-dried and ground into fine powder with a mortar.

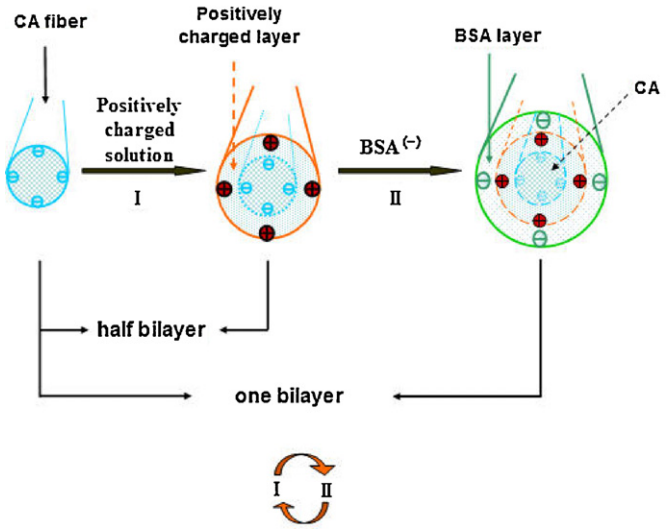

Fig. 1. Schematic diagram illustrating the fabrication of multi-layered CS/BSA or CS–OREC/BSA films on CA fibers via electrostatic LBL deposition.

2.3. Electrospinning of CA fibrous mats

CA mats were fabricated from 17 wt% CA solution prepared with 2/1 (w/w) acetone/*N*,*N*-dimethylacetamide mixture solvent. The CA solution was placed in a plastic syringe which connected to a metal needle tip. The syringe was driven by a syringe pump (LSP02-1B, Baoding Longer Precision Pump Co., Ltd., China). The positive electrode of a high voltage power supply (DW-P303-1ACD8, Tianjin Dongwen High Voltage Co., China) was clamped to the tip of the syringe. A grounded cylindrical collector covered by aluminum foil was rotated with a linear velocity of 100 m/min. The applied voltage was 16 kV, and the tip-to-collector distance was 20 cm. The ambient temperature and relative humidity were maintained at 25 °C and 40%, respectively. Then the prepared fibrous mats were dried at 80 °C to remove the trace solvents under vacuum.

2.4. Preparation of dipping solutions for LBL modification

The concentration of the positively charged chitosan or chitosan–OREC (12/1, w/w) solutions was fixed as 1 mg/mL by dissolving them in a 0.002 M aqueous acetic acid solution and the pH of solutions was controlled at 5. The negatively charged BSA solution was 1 mg/mL in pure water and the pH was adjusted to 6.5. The ionic strength of all dipping solutions was regulated by the addition of NaCl at a concentration of 0.1 M (Deng et al., 2010; Deng, Wang, et al., 2011; Ding, Li, Fujita, & Shiratori, 2006a).

2.5. Fabrication of LBL structured multilayer on CA fibrous mats

The concept for fabrication of LBL structured fibrous mats was shown in Fig. 1. First, CA fibrous mats were immersed into chitosan or intercalated chitosan–OREC suspensions for 20 min, followed by 2 min of rinsing in three pure water baths. The mats were then immersed into the BSA solution for 20 min, followed by the identical rinsing steps. The adsorption and rinsing steps were repeated until the desired number of deposition bilayers was obtained. Here, $(\text{chitosan–OREC/BSA})_n$ was used as a formula to label the LBL structured films, where n was the number of the chitosan–OREC/BSA bilayers. The outermost layer was chitosan–OREC composite when n equaled to 5.5 and 10.5. The LBL films coated fibrous mats were dried at 80 °C for 24 h under vacuum before further characterizations.

2.6. Characterization

Scanning electron microscopy (SEM) and energy-dispersive X-ray (EDX) spectroscopy images were obtained by QUANTA 200 (Philips-FEI, Holland). The diameters of the fibers were measured using image analyzer (Adobe Photoshop 7.0). Fourier transform infrared (FT-IR) spectra were recorded by Nicolet170-SX (Thermo Nicolet Ltd., USA). The small angle X-ray diffraction (SAXRD) was performed on type D/max-rA diffractometer (Rigaku Co., Japan) with Cu target and Ka radiation ($\lambda = 0.154$ nm). The surface elemental composition of the samples was identified by X-ray photoelectron spectroscopy (XPS) using an axis ultra DLD apparatus (Kratos, UK).

2.7. Determination of BSA encapsulation efficiency

After the BSA-loaded fibrous mats were taken out, the BSA remained in the solution was determined via Coomassie Brilliant Blue method to determine the amounts of BSA encapsulated on UV-1800 spectrophotometry (Shimadzu, Japan) at 595 nm, and the initial concentration (1 mg/mL) was used as the control. All the experiments were done in triplicate and mean values were reported. The BSA encapsulation efficiency in the beads was calculated from:

$$\text{EE}\ (\%) = \frac{A - B}{A} \times 100\% \quad (1)$$

where A is the total amount of the BSA given and B is the amount of the BSA lost.

2.8. BSA release from the composite fibrous mats

The BSA release test was conducted in 0.1 M HCl (pH 1.2) and PBS (pH 7.4) for a certain period (Shi et al., 2005; Wang et al., 2010). LBL films coated fibrous mats (100 mg) were put into a conical flask containing 100 mL of the above solution, and then incubated on a constant temperature shaking bed at 37 °C and 100 rpm. After specific intervals, 1 mL of medium was withdrawn and immediately replaced with the same amount of fresh medium. Coomassie Brilliant Blue was used to determine the amounts of BSA released on UV-1800 spectrophotometry at 595 nm. The sample from the non-loaded BSA fibrous mats was taken as the control. All experiments were done in triplicate and mean values were reported.

3. Results and discussion

3.1. Chitosan/BSA multilayer modified CA fibrous mats

Generally, the typically electrospun fibrous mats have a 3D structure with pores in micro and sub-micro size (Ding, Kimura, Sato, Fujita, & Shiratori, 2004; Ding, Li, Miyauchi, Kuwaki, & Shiratori, 2006b; Ji et al., 2006; Lee, Kim, Chen, Shao-Horn, & Hammond, 2009; Yang, Tao, Pang, & Siu, 2008). The deposition space among the fibrous mats is limited and different from that of the other flat substrates, so the optimization of the LBL deposition parameters, such as the number of coating bilayers, the variation of outmost layer and the composition of the coating bilayers, is necessary for the deposition of uniform LBL films on the surface of fibers.

Fig. 2a shows the FE-SEM images of as-spun CA mats containing loosely packed cylindrical fibers with the average fiber diameter of 578 ± 193 nm. Some junctions among the CA fibers were caused by the evaporation of the trace remained solvent after electrospinning, which would dissolve the edge of cellulose acetate fibers. In order to investigate the influence of the number of coating bilayers and the composition of the outmost layer on the formation of LBL films coated fibers, the CA fibers were coated with different numbers of chitosan/BSA bilayers. The morphology of the as-prepared samples is shown in Fig. 2b–e. It could be seen that all the samples still remained fibrous 3D structure after LBL deposition. The morphology was with no obvious difference between 5 and 5.5, or 10 and 10.5 bilayers coated mats, but doubling the bilayers showed slightly thicker deposition as observed in FE-SEM images. Compared with CA mats, BSA loaded fibrous mats displayed more spindle-like beads with large diameter should be attributed to the adsorption of BSA on the surface of fibers and the crosslinking interaction via electrostatic interaction between BSA and chitosan. For chitosan/BSA films coating, the average diameter of $(\text{chitosan/BSA})_{5.5}$ and $(\text{chitosan/BSA})_{10}$ films coating was 643 and 707 nm, respectively. Besides, doubling the number of coating bilayers presented not only thicker deposition, but also more bundles and bigger junctions as observed from FE-SEM images (Deng et al., 2010). In addition, compared with the smooth surface of the CA fibers, the LBL films coated fibers showed high surface roughness containing protuberances, which was caused by the different dispersion speed of deposition materials into various sites in the space-limited 3D structure (Ding et al., 2006a). In conclusion, the number of coating bilayers was important in the formation and morphology of LBL films-coated fibrous mats.

Table 1
ζ-Potential (mV) of OREC, CS, BSA, CA and CS–OREC composites (12/1).

Samples	OREC	CS	BSA	CA	CS–OREC
ζ-Potential (mV)	+24.2	+36.1	−10.0	−28.4	+42.8

3.2. OREC-containing coating bilayers modified CA fibrous mats

Intercalated chitosan–OREC solution was selected as positively charged deposition materials to coat the surface of CA fibers. FE-SEM images of fibrous CA mats coated with 5, 5.5, 10 and 10.5 chitosan–OREC/BSA bilayers were shown in Fig. 3. The incorporation of OREC into LBL dipping solutions showed a remarkable expansion in the average diameter of LBL films coated mats from 644 ($n = 5$) to 730 nm ($n = 10$). Besides, more junctions, denser bundles and much bigger protuberances were formed in the chitosan–OREC/BSA films coated mats than those in the chitosan/BSA films coated samples. In addition, the diameter distribution of fibers was inhomogeneous among Fig. 3a and b with much more ultra-thin fibers, while in Fig. 3c and d, as the number of bilayers increased, the number of thin fibers reduced and the distribution of diameters tended to be homogeneous.

The results above might be attributed to the higher positive charge (+42.8 mV), larger interlayer distance and the resultant enlarged surface area to volume ratio of chitosan–OREC composites. In Table 1, chitosan and chitosan–OREC composites have ζ-potential value of +36.1 and +42.8 mV, respectively. The intercalated chitosan–OREC composite with higher positive charge could result in more deposition of chitosan–OREC on negatively charged CA mats and more adsorption of BSA through electrostatic interactions. Therefore, in the first step of LBL process, more and thicker chitosan–OREC could be assembled on CA fibers than chitosan itself, which would adsorb more BSA in the next step. Thus, LBL films containing OREC was thicker than that of films without OREC. As a result, the morphology of LBL films coated mats was greatly affected by the addition of OREC.

EDX spectrum was performed to confirm the expected compositions on $(\text{chitosan–OREC/BSA})_{10.5}$ films coated fibrous mats (Fig. 3e). The characteristic peaks of Si and Al elements in the spectrum were identified. As is known, the main components of OREC include Si, Al, and Na elements. Na element was resulted from SDS

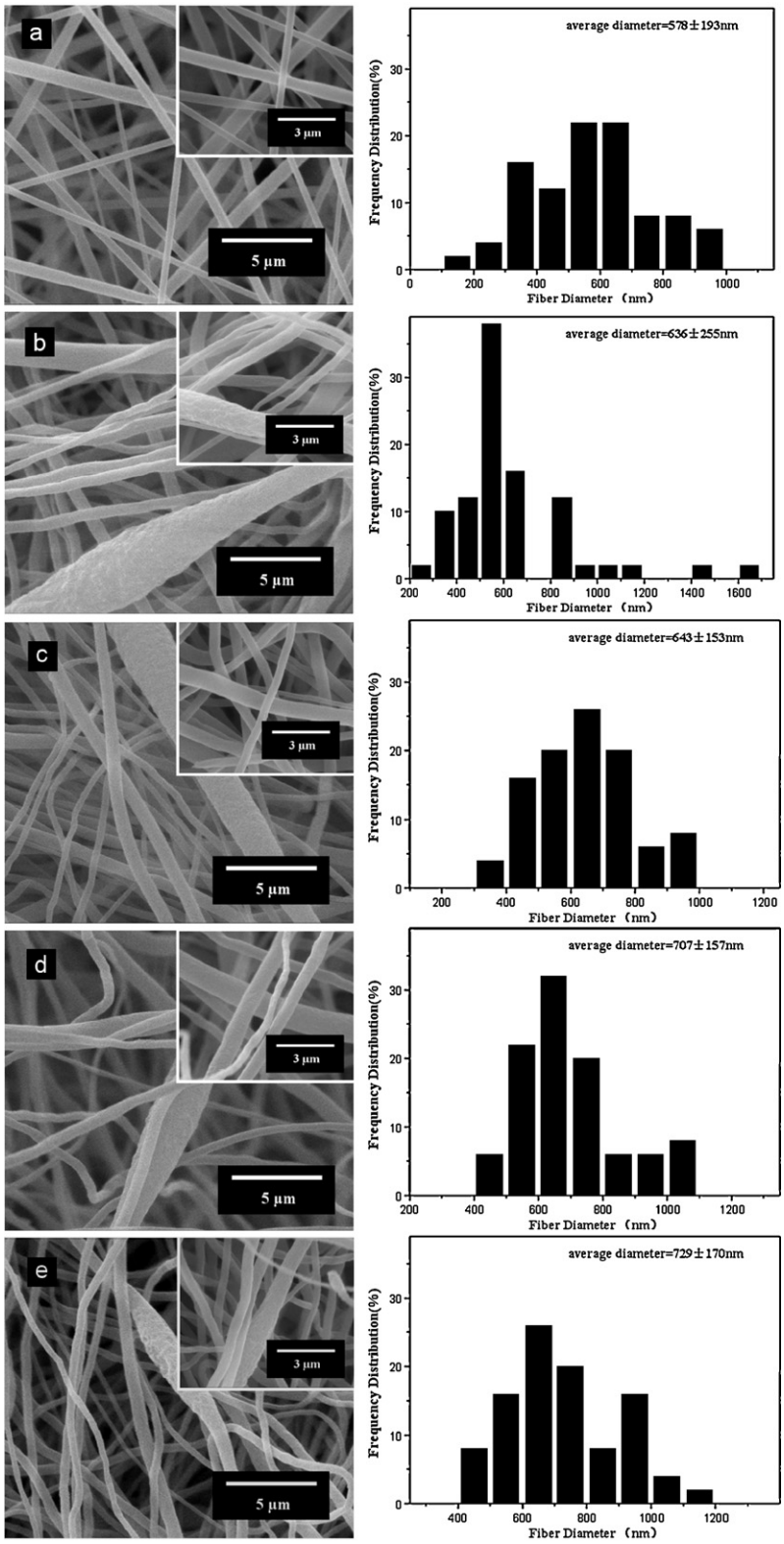

Fig. 2. FE-SEM images and fiber diameter distribution of (a) CA fibrous mats and LBL structured mats coated with: (b) $(CS/BSA)_5$, (c) $(CS/BSA)_{5.5}$, (d) $(CS/BSA)_{10}$ and (e) $(CS/BSA)_{10.5}$.

during the modification of REC to OREC or the addition of NaCl in the regulation of the ionic strength of all dipping solutions. The EDX results indicated that OREC was successfully assembled onto the surface of CA fibrous mats.

To investigate the structure of predesigned intercalated architecture in LBL films, the SAXRD patterns of fibrous samples were recorded (Fig. 4). The SAXRD curves for chitosan, BSA powder and $(chitosan/BSA)_{10.5}$ films-coated fibers showed no obvious difference with each other. The curve for OREC presented the corresponding azimuthally averaged radial intensity trace. The maximum intensity is located at $2\theta = 3.60^\circ$, which corresponds to a mean correlation distance between

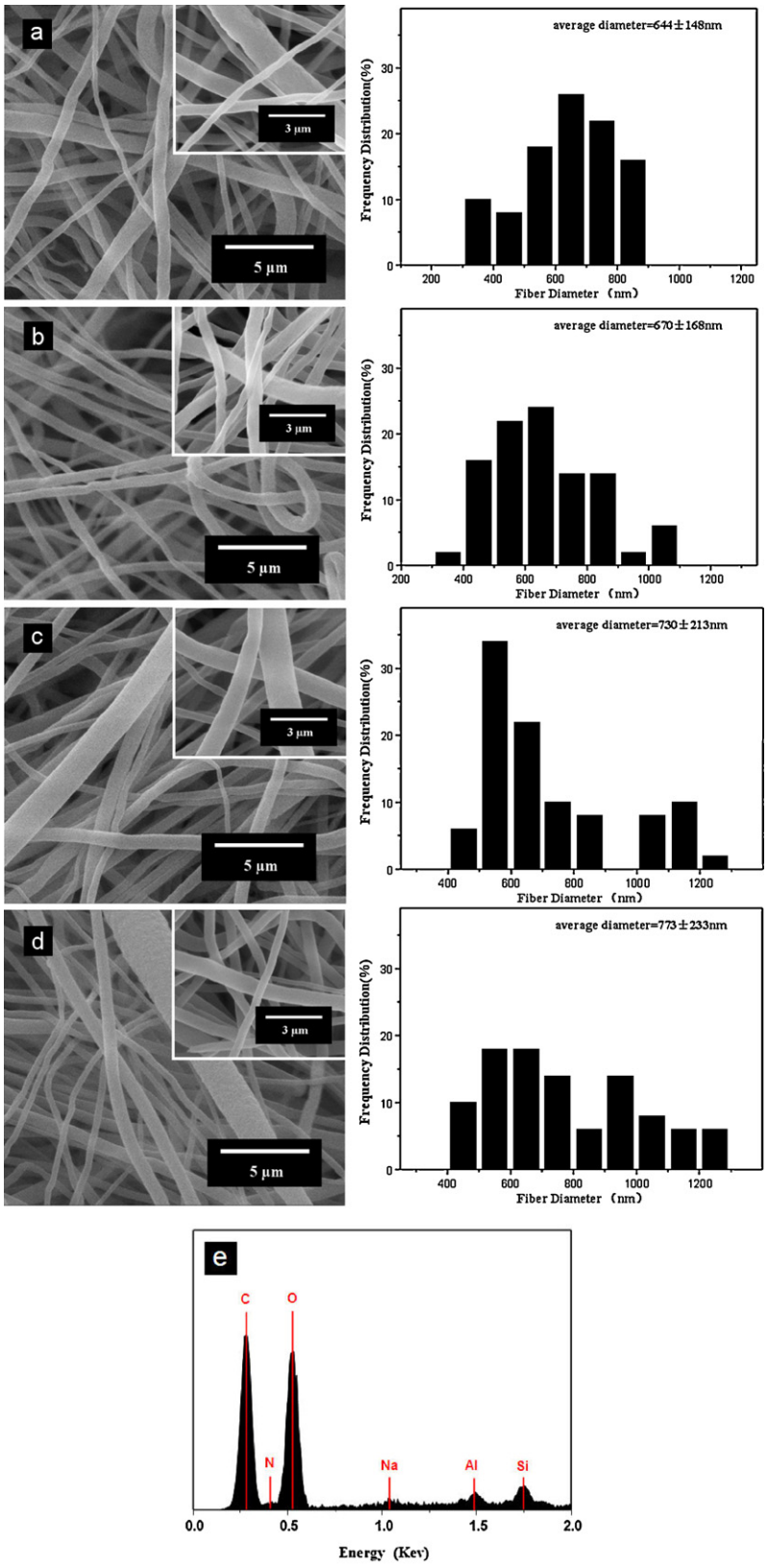

Fig. 3. FE-SEM images and fiber diameter distribution of LBL structured mats coated with: (a) $(CS–OREC/BSA)_5$, (b) $(CS–OREC/BSA)_{5.5}$, (c) $(CS–OREC/ALG)_{10}$, (d) $(CS–OREC/ALG)_{10.5}$ and (e) EDX spectrum of selected area of $(CS–OREC/BSA)_{10.5}$ films coated fibrous mats.

the interlayer of OREC of 2.45 nm, as calculated by Bragg's equation:

$$2d \sin\theta = n\lambda \quad (2)$$

where d is the interlayer spacing, θ is the angle of incidence, λ is wave length, and n is an integer, the order of the reflection. Fig. 4b shows the SAXRD pattern of $(chitosan–OREC/BSA)_{10.5}$ films deposited mats. The spacing distance between OREC interlayer was

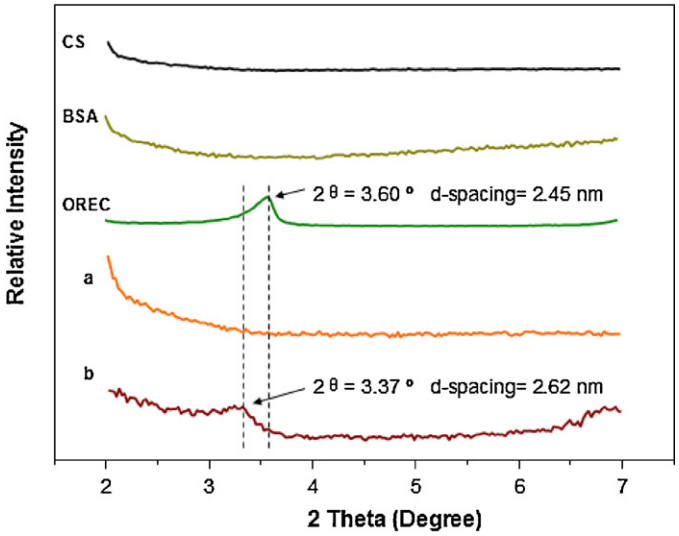

Fig. 4. SAXRD patterns of CS, BSA and OREC powder and LBL structured fibrous mats coated with (a) $(CS/BSA)_{10.5}$ and (b) $(CS–OREC/BSA)_{10.5}$.

enlarged to 2.62 nm. Compared with that of OREC, the SAXRD curve of $(chitosan–OREC/BSA)_{10.5}$ films coating diminished, representing the enlarged interlayer distance of OREC, which confirmed that chitosan chains were successfully inserted into the interlayer of OREC.

XPS scans were recorded to further verify the surface composition of resultant samples. Fig. 5 shows the XPS data of as-spun CA mats, $(chitosan/BSA)_{10}$ and $(chitosan–OREC/BSA)_{10.5}$ films coated samples. For CA mats (Fig. 5a), the carbon and oxygen peaks were observed. After the $(chitosan/BSA)_{10}$ and $(chitosan–OREC/BSA)_{10.5}$ films deposition, the new nitrogen peak (N 1s) at 397.5 eV was detected in both Fig. 5b and c. Additionally, the characteristic peak of Si2p at 99.5 eV and Al 2p at 72.2 eV could be observed in Fig. 5c, which corresponded to the previous results, confirming the existence of OREC in the surface of $(chitosan–OREC/BSA)_{10.5}$ films coating.

3.3. Determination of BSA encapsulation efficiency

The BSA loss in the washing steps and the BSA loading capacity of the LBL structured samples is shown in Fig. 6. During the washing steps in LBL process, the amount of the BSA loss should be considered. Indeed, the BSA would be lost when the LBL films coated mats were immersed in the three washing baths. It was easy to observe that the loss of BSA in the first washing cup was higher than that in the second and third cups, and the second was also higher than the third. Besides, doubling the coating bilayers needed doubling washing steps, and the amount of BSA loss would be increased. In addition, when OREC was assembled on the surface of the fibers, the degree of BSA loss could be inhibited. This might be because of the increased positive charge, enlarged interlayer distance as well as the higher surface area to volume ratio due to the addition of OREC, which might cause efficient contact and interaction with more protein.

For the same reason, the LBL films containing OREC coated mats also showed higher protein loading capacity at 55.3 mg/g compared to those without OREC at 51.3 mg/g when $n = 5$ or 5.5. Besides, doubling the bilayers resulted in a slight growth in the BSA loading capacity. The more number of bilayers was coated, the more BSA would be loaded. Moreover, the BSA loading capacity was also enlarged from 57.1 to 61.2 mg/g for $(chitosan/BSA)_{10/10.5}$ and $(chitosan–OREC/BSA)_{10/10.5}$ films coating, respectively, which

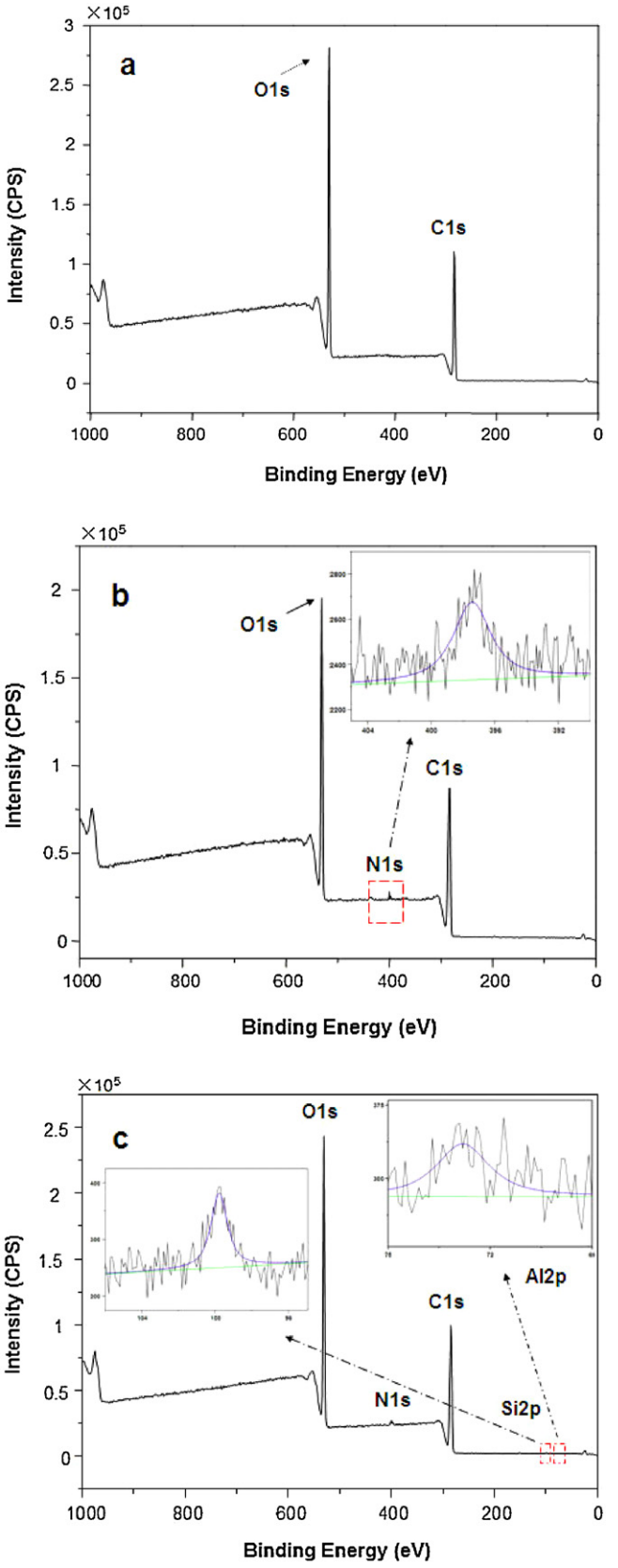

Fig. 5. XPS peak fitting curves of: (a) CA fibrous mats, (b) $(CS/BSA)_{10}$ films coated fibrous mats and (c) $(CS–OREC/BSA)_{10.5}$ films coated mats.

Table 2
Release profiles of BSA in pH 1.2 HCl and in pH 7.4 PBS from the LBL structured fibrous mats. All data shown are the mean ± standard deviations ($n = 3$).

Samples coated with LBL films	Release profiles of BSA in pH 1.2 HCl over different period			
	1 h	2 h	4 h	8 h
$(CS/BSA)_5$	27.47 ± 0.57%	31.9 ± 0.63%	42.7 ± 0.71%	45.5 ± 1.02%
$(CS/BSA)_{5.5}$	27.59 ± 0.65%	34.8 ± 1.05%	42.8 ± 0.82%	44.1 ± 0.98%
$(CS/BSA)_{10}$	24.81 ± 0.59%	31.7 ± 0.80%	41.5 ± 0.68%	40.2 ± 0.99%
$(CS/BSA)_{10.5}$	25.3 ± 0.82%	32.3 ± 0.46%	40.6 ± 0.96%	43.4 ± 0.87%
$(CS–OREC/BSA)_5$	26.8 ± 0.80%	35.7 ± 0.82%	46.4 ± 0.78%	47.9 ± 0.88%
$(CS–OREC/BSA)_{5.5}$	26.8 ± 0.75%	32.0 ± 0.97%	46.8 ± 0.99%	49.0 ± 1.05%
$(CS–OREC/BSA)_{10}$	22.4 ± 0.81%	32.0 ± 0.69%	37.3 ± 0.63%	38.2 ± 0.94%
$(CS–OREC/BSA)_{10.5}$	23.1 ± 0.99%	26.8 ± 0.38%	40.7 ± 0.80%	42.4 ± 1.09%
Samples coated with LBL films	Release profiles of BSA in pH 7.4 PBS over different period			
	1 h	2 h	4 h	8 h
$(CS/BSA)_5$	34.30 ± 0.75%	42.47 ± 0.92%	63.70 ± 0.75%	74.27 ± 1.20%
$(CS/BSA)_{5.5}$	38.72 ± 0.83%	50.09 ± 1.23%	69.69 ± 0.38%	79.03 ± 1.33%
$(CS/BSA)_{10}$	33.41 ± 0.62%	49.95 ± 1.01%	59.91 ± 0.79%	63.76 ± 1.18%
$(CS/BSA)_{10.5}$	34.44 ± 0.43%	52.56 ± 1.05%	63.28 ± 0.81%	65.34 ± 1.09%
$(CS–OREC/BSA)_5$	34.70 ± 0.79%	51.88 ± 0.39%	62.88 ± 1.21%	79.68 ± 1.39%
$(CS–OREC/BSA)_{5.5}$	35.76 ± 0.91%	50.53 ± 0.97%	67.37 ± 1.33%	82.12 ± 1.72%
$(CS–OREC/BSA)_{10}$	31.26 ± 0.83%	43.54 ± 0.82%	57.50 ± 0.92%	72.47 ± 1.22%
$(CS–OREC/BSA)_{10.5}$	32.94 ± 0.70%	49.33 ± 0.62%	61.81 ± 1.20%	74.90 ± 1.41%

further verified that adding OREC could enhance the protein loading capacity of the LBL structured fibrous mats.

3.4. In vitro cumulative release profiles of BSA

Table 2 presents the cumulative release profiles of BSA in different LBL structured mats in the simulative gastrointestinal tract. As the time increased, the release rate of BSA of all the samples gradually went up to the maximum data within 8 h. This initial release could be related to the diffusion of the protein caused by mats swelling and also the release of the protein adsorbed toward the surface of the matrix (Wang, Du, Luo, Lin, & Kennedy, 2007). In the pH-gradient release assay, only a small amount of BSA was released from the mats in 1 h, and 8 h later the cumulative amount was only around 38–50% due to the gradually reduced cumulative rate when the pH was 1.2. However, when pH was 7.4, a larger amount of BSA (between 31% and 39%) was released within 1 h and 62–84% BSA released into PBS buffer after 8 h because of the quick dissociation of the delivery systems. In addition, as for the samples with identical number of bilayers and record time, obvious increasing of the release amount could be seen in pH 7.4, in comparison with pH 1.2.

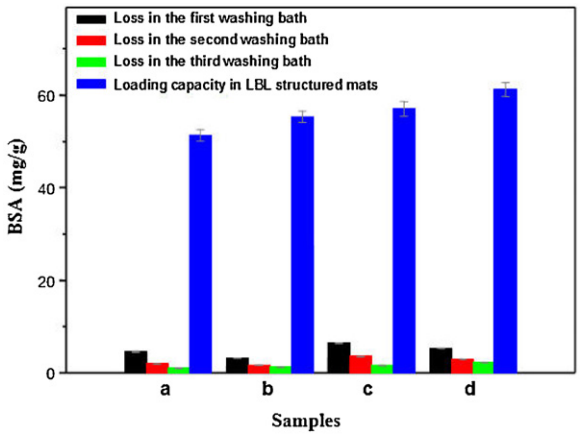

Fig. 6. The BSA loss in the washing steps and the BSA loading capacity of LBL structured fibrous mats coated with: (a) $(CS/BSA)_5$ or $(CS/BSA)_{5.5}$, (b) $(CS–OREC/BSA)_5$ or $(CS–OREC/BSA)_{5.5}$, (c) $(CS/BSA)_{10}$ or $(CS/BSA)_{10.5}$ and $(CS–OREC/BSA)_{10}$ or $(CS–OREC/BSA)_{10.5}$. All data shown are the mean ± standard deviations ($n = 3$).

The results might be attributed to the increased hydrophobicity and electrostatic attractive forces in pH 1.2 (Liu, Li, Zhao, De Yao, & Liu, 2002; Perugini, Genta, Conti, Modena, & Pavanetto, 2003), which could inhibit the protein from fast release and thus improve the controlled release properties. However, the gradual deprotonation of chitosan or chitosan–OREC in pH 7.4 weakened the extent of the interactions inside the mats. Thereupon, soluble BSA could be brought into the solution (Gonzalez-Rodriguez et al., 2002).

Besides, doubling bilayers film-coated mats generally showed lower release rate than those coated with 5 or 5.5 layers at both pH 1.2 and 7.4. According to the previous results (Fig. 6), the remarkably enlarged loading capacity of the doubling bilayers coated mats due to the thicker structure, but might make an adverse effect on the release efficiency of protein and prevent the protein from diffusing into the medium rapidly. Meanwhile, it was slightly distinguishable between 5 and 5.5 as well as 10 and 10.5 bilayers. The samples with BSA in the outmost layer showed unobviously lower than those with chitosan or chitosan–OREC as the outmost layer in release efficiency, it was most likely that amino and hydroxyl groups in chitosan would form hydrogen bond with solutions, which resulted in promoting the solutions penetrating into the mats, and BSA in the mats diffusing easily into the solution.

Interestingly, it can be seen that protein release of the chitosan–OREC/BSA films coated mats remarkably increased compared with that of chitosan/BSA films coated mats either at pH 1.2 or 7.4. This might because chitosan–OREC/BSA films coating had more compact structure than chitosan/BSA films coating, and the layered structure of OREC could promote the medium to permeate into the mats and BSA in the mats diffuse easily into the medium (Xu et al., 2012). In addition, mats with larger distance between the interlayer of OREC and increased specific surface area might boost the release of BSA. Therefore, the fact verified that the release speed of protein was affected by the addition of OREC.

In conclusion, the $(chitosan–OREC/BSA)_{5.5}$ coated CA fibrous mats in pH 7.4 PBS buffer presented the optimal release efficiency of protein in the initial 8 h, while the $(chitosan/BSA)_{10}$ films coating in pH 1.2 showed the lowest efficiency in protein release for this short time. The release of protein in the initial 8 h could be controlled by adjusting the number of deposition bilayers, the outmost layer and the composition of coating bilayers.

4. Conclusion

LBL structured fibrous mats with intercalation structure were successfully fabricated via solution intercalation method, electrospinning and electrostatic LBL self-assembly technique. The morphology, intercalated structure, surface elements, and protein controlled release properties were investigated systematically. The conclusions could be obtained as follows:

1. The morphology of LBL films coated fibrous mats could be greatly influenced by deposition conditions. The resultant samples still maintained prefect fiber shape and 3D structure. The EDX and XPS results demonstrated that OREC and chitosan were assembled on the surface of the fibers. The SAXRD data showed that OREC was intercalated by chitosan chains and the interlayer distance of OREC was enlarged.
2. The incorporation of OREC into LBL films modified mats could affect the protein encapsulation capacity and protein release efficiency. The release of protein in the initial time could be controlled by adjusting the number of deposition bilayers, the outmost layer and the composition of coating bilayers. Besides, the developed approach to immobilize layered silicate and protein onto polymer fibers with controllable thickness and enlarged interlayer distance might also be utilized to tailor the sizes, compositions, and surface properties of other 3D LBL structured materials for various applications such as catalysis, sensors, tissue engineering, food packaging and antimicrobial wound dressing.

Acknowledgements

This project was supported by the National Natural Science Fund (Nos. 31101365, 81000597 and 81070248) and was partially supported by the Fundamental Research Funds for the Central Universities of China (No. 52902-0900202208).

References

Bhattarai, N., Edmondson, D., Veiseh, O., Matsen, F. A., & Zhang, M. Q. (2005). Electrospun chitosan-based nanofibers and their cellular compatibility. *Biomaterials*, *26*, 6176–6184.

Darder, M., Colilla, M., & Ruiz-Hitzky, E. (2003). Biopolymer–clay nanocomposites based on chitosan intercalated in montmorillonite. *Chemistry of Materials*, *15*, 3774–3780.

Decher, G., & Hong, J. D. (1991). Buildup of ultrathin multilayer films by a self-assembly process: II. Consecutive adsorption of anionic and cationic bipolar amphiphiles and polyelectrolytes on charged surfaces. *Berichte der Bunsen-Gesellschaft Physical Chemistry Chemical Physics*, *95*, 1430–1434.

Deng, H. B., Li, X. Y., Ding, B., Du, Y. M., Li, G. X., Yang, J. H., et al. (2011). Fabrication of polymer/layered silicate intercalated nanofibrous mats and their bacterial inhibition activity. *Carbohydrate Polymers*, *83*, 973–978.

Deng, H. B., Lin, P. H., Xin, S. J., Huang, R., Li, W., Du, Y. M., et al. (2012). Quaternized chitosan-layered silicate intercalated composites based nanofibrous mats and their antibacterial activity. *Carbohydrate Polymers*, *89*, 307–313.

Deng, H. B., Wang, X. Y., Liu, P., Ding, B., Du, Y. M., Li, G. X., et al. (2011). Enhanced bacterial inhibition activity of layer-by-layer structured polysaccharide film-coated cellulose nanofibrous mats via addition of layered silicate. *Carbohydrate Polymers*, *83*, 239–245.

Deng, H. B., Zhou, X., Wang, X. Y., Zhang, C. Y., Ding, B., Zhang, Q. H., et al. (2010). Layer-by-layer structured polysaccharides film-coated cellulose nanofibrous mats for cell culture. *Carbohydrate Polymers*, *80*, 474–479.

Ding, B., Fujimoto, K., & Shiratori, S. (2005). Preparation and characterization of self-assembled polyelectrolyte multilayered films on electrospun nanofibers. *Thin Solid Films*, *491*, 23–28.

Ding, B., Kimura, E., Sato, T., Fujita, S., & Shiratori, S. (2004). Fabrication of blend biodegradable nanofibrous nonwoven mats via multi-jet electrospinning. *Polymer*, *45*, 1895–1902.

Ding, B., Li, C. R., Fujita, S., & Shiratori, S. (2006). Layer-by-layer self-assembled tubular films containing polyoxometalate on electrospun nanotibers. *Colloids and Surfaces A: Physicochemical and Engineering Aspects*, *284*, 257–262.

Ding, B., Li, C. R., Miyauchi, Y., Kuwaki, O., & Shiratori, S. (2006). Formation of novel 2D polymer nanowebs via electrospinning. *Nanotechnology*, *17*, 3685–3691.

Gonzalez-Rodriguez, M. L., Holgado, M. A., Sanchez-Lafuente, C., Rabasco, A. M., & Fini, A. (2002). Alginate/chitosan particulate systems for sodium diclofenac release. *International Journal of Pharmaceutics*, *232*, 225–234.

Ji, Y., Ghosh, K., Shu, X. Z., Li, B. Q., Sokolov, J. C., Prestwich, G. D., et al. (2006). Electrospun three-dimensional hyaluronic acid nanofibrous scaffolds. *Biomaterials*, *27*, 3782–3792.

Lee, S. W., Kim, B. S., Chen, S., Shao-Horn, Y., & Hammond, P. T. (2009). Layer-by-layer assembly of all carbon nanotube ultrathin films for electrochemical applications. *Journal of the American Chemical Society*, *131*, 671–679.

Liu, W. G., Li, F., Zhao, X. D., De Yao, K., & Liu, Q. G. (2002). Atom force microscopic characterisation of the interaction forces between bovine serum albumin and cross-linked alkylated chitosan membranes in media of different pH. *Polymer International*, *51*, 1459–1463.

Ma, G. P., Liu, Y., Peng, C., Fang, D. W., He, B. J., & Nie, J. (2011). Paclitaxel loaded electrospun porous nanofibers as mat potential application for chemotherapy against prostate cancer. *Carbohydrate Polymers*, *86*, 505–512.

Perugini, P., Genta, I., Conti, B., Modena, T., & Pavanetto, F. (2003). Periodontal delivery of ipriflavone: New chitosan/PLGA film delivery system for a lipophilic drug. *International Journal of Pharmaceutics*, *252*, 1–9.

Shi, X. W., Du, Y. M., Sun, L. P., Yang, J. H., Wang, X. H., & Su, X. L. (2005). Ionically crosslinked alginate/carboxymethyl chitin beads for oral delivery of protein drugs. *Macromolecular Bioscience*, *5*, 881–889.

Tiwari, S. K., Tzezana, R., Zussman, E., & Venkatraman, S. S. (2010). Optimizing partition-controlled drug release from electrospun core–shell fibers. *International Journal of Pharmaceutics*, *392*, 209–217.

Wang, X. Y., Du, Y. M., Luo, J. W., Lin, B. F., & Kennedy, J. F. (2007). Chitosan/organic rectorite nanocomposite films: Structure, characteristic and drug delivery behaviour. *Carbohydrate Polymers*, *69*, 41–49.

Wang, X. Y., Du, Y. M., Luo, J. W., Yang, J. H., Wang, W. P., & Kennedy, J. F. (2009). A novel biopolymer/rectorite nanocomposite with antimicrobial activity. *Carbohydrate Polymers*, *77*, 449–456.

Wang, X. Y., Du, Y. M., Yang, H. H., Wang, X. H., Shi, X. W., & Hu, Y. (2006). Preparation, characterization and antimicrobial activity of chitosan/layered silicate nanocomposites. *Polymer*, *47*, 6738–6744.

Wang, X. Y., Pei, X. F., Du, Y. M., & Li, Y. (2008). Quaternized chitosan/rectorite intercalative materials for a gene delivery system. *Nanotechnology*, 19.

Wang, S. H., Shi, X. Y., Chen, X. S., & Baker, J. R. (2009). Therapeutic efficacy of 2-methoxyestradiol microcrystals encapsulated within polyelectrolyte multilayers. *Macromolecular Bioscience*, *9*, 429–436.

Wang, X. Y., Tang, Y. F., Li, Y., Zhu, Z., & Du, Y. M. (2010). The rheological behaviour and drug-delivery property of chitosan/rectorite nanocomposites. *Journal of Biomaterials Science-Polymer Edition*, *21*, 171–184.

Wu, F., & Jin, T. (2008). Polymer-based sustained-release dosage forms for protein drugs, challenges, and recent advances. *AAPS PharmSciTech*, *9*, 1218–1229.

Xu, R., Feng, X., Li, W., Xin, S., Wang, X., Deng, H., et al. (2012). Novel polymer-layered silicate intercalated composite beads for drug delivery. *Journal of Biomaterials Science, Polymer Edition*, http://dx.doi.org/10.1163/156856211X619630

Yang, A., Tao, X. M., Pang, G. K. H., & Siu, K. G. G. (2008). Preparation of porous tin oxide nanobelts using the electrospinning technique. *Journal of the American Ceramic Society*, *91*, 257–262.

Zhang, L., Guo, J., Peng, X. H., & Jin, Y. (2004). Preparation and release behavior of carboxymethylated chitosan/alginate microspheres encapsulating bovine serum albumin. *Journal of Applied Polymer Science*, *92*, 878–882.